

## Learning to Diagnose Privately: DP-Powered LLMs for Radiology Report Classification

*Payel Bhattacharjee<sup>1</sup>, Fengwei Tian<sup>1</sup>, Geoffrey D. Rubin<sup>2</sup>, Joseph Y. Lo<sup>3</sup>, Nirav Merchant<sup>4</sup>, Heidi Hanson<sup>5</sup>, John Gounley<sup>5</sup>, Ravi Tandon<sup>1</sup>*

**Purpose:** This study proposes a framework for fine-tuning large language models (LLMs) with differential privacy (DP) to perform multi-abnormality classification on radiology report text. By injecting calibrated noise during fine-tuning, the framework seeks to mitigate the privacy risks associated with sensitive patient data and protect against data leakage while maintaining classification performance.

**Materials and Methods:** We used 50,232 radiology reports from the publicly available MIMIC-CXR chest radiography and CT-RATE computed tomography datasets, collected between 2011 and 2019. Fine-tuning of LLMs was conducted to classify 14 labels from MIMIC-CXR dataset, and 18 labels from CT-RATE dataset using Differentially Private Low-Rank Adaptation (DP-LoRA) in high and moderate privacy regimes (across a range of privacy budgets  $\epsilon = \{0.01, 0.1, 1.0, 10.0\}$ ). Model performance was evaluated using weighted F1 score across three model architectures: BERT-medium, BERT-small, and ALBERT-base. Statistical analyses compared model performance across different privacy levels to quantify the privacy-utility trade-off.

**Results:** We observe a clear privacy-utility trade-off through our experiments on 2 different datasets and 3 different models. Under moderate privacy guarantees the DP fine-tuned models achieved weighted F1 scores of 0.88 on MIMIC-CXR and 0.59 on CT-RATE, compared to non-private LoRA baselines of 0.90 and 0.78, respectively.

---

<sup>1</sup> (payelb@arizona.edu, fengtian@arizona.edu, tandonr@arizona.edu) Department of Electrical and Computer Engineering, University of Arizona, Tucson, AZ

<sup>2</sup> (grubin@arizona.edu) Department of Radiology & Imaging Sciences, University of Arizona, Tucson, AZ

<sup>3</sup> (joseph.lo@duke.edu) Departments of Radiology and Electrical and Computer Engineering, Duke University, Durham, NC

<sup>4</sup> (nirav@arizona.edu) Data Science Institute, University of Arizona, Tucson, AZ

<sup>5</sup> (hansonha@ornl.gov, gounleyjp@ornl.gov) Oak Ridge National Laboratory, Oak Ridge, TN

**Conclusion:** Differentially private fine-tuning using LoRA enables effective and privacy-preserving multi-abnormality classification from radiology reports, addressing a key challenge in fine-tuning LLMs on sensitive medical data.

**Keywords:** *Privacy Preserving Large Language Models, multi-abnormality classification, radiology reports, Chest radiography, computed tomography, Differential Privacy.*

**Key Results:**

Demonstrated privacy vulnerabilities in LLMs for healthcare by performing memorization attacks on GPT-2 and BERT models in multi-abnormality classification tasks.

- Applied DP-LoRA, a differentially private fine-tuning framework, to classify free-text chest X-ray reports while ensuring formal privacy guarantees.
- Achieved predictive performance comparable to non-private models on MIMIC-CXR and CT-RATE datasets, even under strong privacy constraints.

**Abbreviations:** **Large Language Model = LLM, Differential Privacy = DP, DP-SGD = Differentially Private Stochastic Gradient Descent, Low Rank Adaptation = LoRA, Differentially Private Fine-tuning = DP-FT.**

**Summary Statement:**

This work provides DP-guarantees [1] [2] during fine-tuning of LLMs using LoRA [3] for multi-abnormality classification from text-radiology reports, striking a balance between predictive performance and protection of sensitive patient information.

**Introduction:**

LLMs are transforming high-stakes fields such as finance [4], education [5], and healthcare [6], [7], where both accuracy and efficiency are critical. These advancements have enabled impactful applications in healthcare, particularly in enhancing report summarization, diagnosis, abnormality classification through both fully and weakly supervised methods [5,6]. LLMs such as BERTSUM [8], and BERT [9] are being used for report summarization and disease classification, whereas domain-specific variants such as BioBERT [10], RadioBERT [11], and ChestXRayBERT [12] have demonstrated strong performance on specialized biomedical and radiology-related tasks. In clinical contexts, fine-tuning LLMs on task-specific, locally sourced, and often private datasets is a common practice to tailor models for specialized downstream applications. For instance, LLMs can help convert free-text radiology reports into structured formats, improving data indexing, clarity, and quality control. They can also generate multi-abnormality labels [13] from reports to annotate corresponding medical images [11], one of the few scalable methods for building large, labeled datasets needed to train robust detection and classification models [14]. These use cases highlight why LLMs are valuable tools. Although medical datasets are typically filtered to remove PHI prior to using them to train or test LLMs, we hypothesize that LLMs may still memorize sensitive details such as rare clinical phrases, verbatim report text, implicit patient identifiers, and structured fields like date or procedures even from anonymized patient reports. This memorization capability poses risks for patient re-identification and unintended disclosure of sensitive medical details using advanced attack techniques such as [15], [16]. The study highlights that even the text completion task given to fine-tuned LLMs can leak private and sensitive information about the training data. A recent study [17] highlights the potential cybersecurity threats and mitigation strategies while using LLMs in healthcare. These prior works motivate and highlight the need for private fine-tuning, a relatively underexplored area in the context of medical report classification. Therefore, fine-tuning large LLMs like ChexBERT, Chexpert, and Vicuna on private medical data raises privacy concerns, motivating recent work on privacy-preserving methods such as DP-OPT [18]. This Study builds on DP-based fine-tuning, adopting DP-Low Rank Adaptation (DP-LoRA) framework that reduces fine-tuning complexity while preserving privacy. To the best of our knowledge, no prior work has incorporated DP-LoRA [19] for multi-abnormality classification from free-text radiology

reports. This paper first examines LoRA-based fine-tuning for multi-abnormality classification on radiology reports in a non-private setting, then incorporates DP-stochastic gradient descent (DP-SGD) [20] to enforce rigorous privacy guarantees during DP-LoRA based fine-tuning.

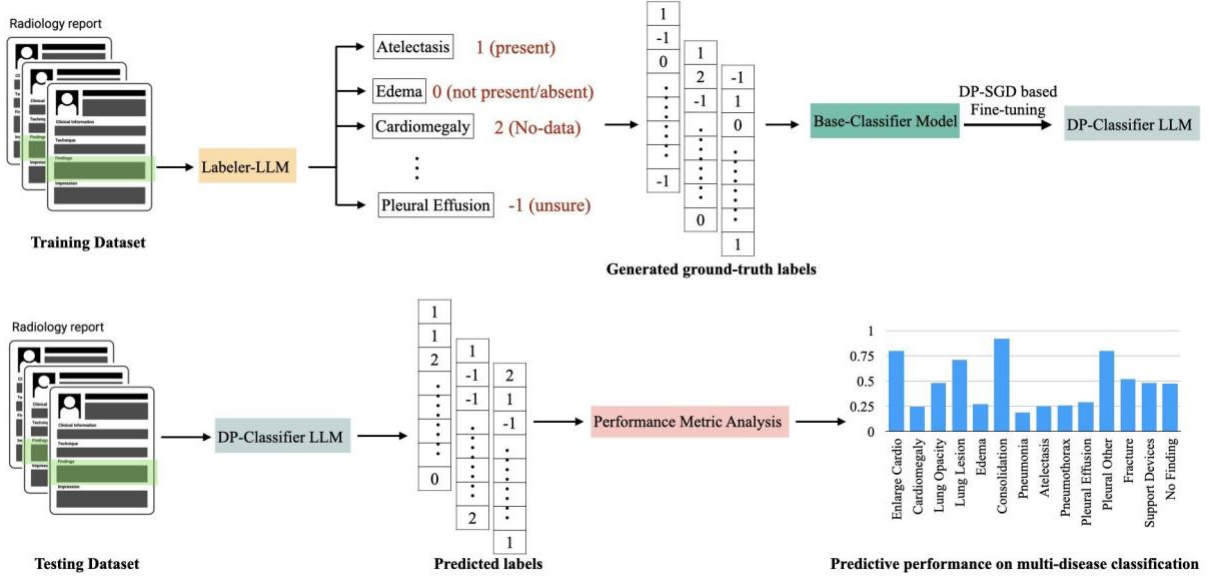


Figure 1: Workflow of the proposed DP fine-tuning framework for multi-abnormality classification problem from the “Findings” of free-text chest radiology reports.

## **Materials and Methods:**

This study utilizes two publicly available free-text radiology based datasets: MIMIC-CXR [21], and CT-RATE dataset [22]. From MIMIC-CXR, 20,883 chest X-ray reports were used for training and 2,610 for testing. For patients with multiple studies, we aggregated all reports to create unified “Findings” and “Impression” sections and removed duplicates. CT-RATE includes 25,692 non-contrast chest CT scans from 21,304 patients, expanded to 50,188 volumes with associated reports and multi-abnormality labels. While both datasets are established benchmarks, to our knowledge, this is the first application of

differentially private fine-tuning (DP-FT) of LLMs for multi-abnormality classification using these corpora.

Our framework is readily extensible to other medical text-based datasets.

**Models and Reference Standard:** Figure 1 illustrates the workflow of our private multi-abnormality classification framework from text-based radiology reports. For MIMIC-CXR, we use ChexBERT [13] to generate labels across 14 classes: *["Enlarged Cardiomeastinum", "Cardiomegaly", "Lung Opacity", "Lung Lesion", "Edema", "Consolidation", "Pneumonia", "Atelectasis", "Pneumothorax", "Pleural Effusion", "Pleural Other", "Fracture", "Support Devices", "No Finding"]*. To focus on disease presence, we binarize the ChexBERT labels by merging unsure (-1) and no data (+2) into the not present (0) class, retaining only present (+1) as positive. For CT-RATE, we use RadBERT [23] model which performs binary classification (present/absent) over 18 classes: *["Medical material", "Arterial wall calcification", "Cardiomegaly", "Pericardial effusion", "Coronary artery wall calcification", "Hiatal hernia", "Lymphadenopathy", "Emphysema", "Atelectasis", "Lung nodule", "Lung opacity", "Pulmonary fibrotic sequela", "Pleural effusion", "Mosaic attenuation pattern", "Peribronchial thickening", "Consolidation", "Bronchiectasis", "Interlobular septal thickening"]*. Figure 2 shows a few representative examples of the reference standard labels generated for MIMIC-CXR and CT-RATE datasets using the report *“Findings”*.

(a) Reference Standard Labels Generated from MIMIC-CXR dataset with ChexBERT Classifier

Report Findings	Enlarged Cardiomeastinum	Cardiomegaly	Lung Opacity	Lung Lesion	Edema	Consolidation	Pneumonia	Atelectasis	Pneumothorax	Pleural Effusion	Pleural Other	Fracture	Support Devices	No Finding
Subtle streaky opacity in the left lower lobe may reflect atelectasis, though infection cannot be entirely excluded. There is no pleural effusion or pneumothorax. There is no central vascular congestion or overt pulmonary edema. Mediastinal and hilar contours are normal. Heart size is normal.	0	0	1	2	0	2	-1	-1	0	0	2	2	2	2
	0	0	1	0	0	0	0	0	0	0	0	0	0	0
Patchy linear opacities at the right base most likely represent atelectasis. There is no definite focal consolidation or pleural effusion or pneumothorax. Cardiomeastinal silhouette is stable with dense calcifications at the thoracic aorta. There is a right chest wall pacemaker with leads terminating in the right atrium and right ventricle. A fracture of the left fourth posterior rib is likely not acute.	-1	2	1	2	2	0	2	1	0	0	2	1	1	2
	0	0	1	0	0	0	0	1	0	0	0	1	1	0

**(b) Reference Standard Labels Generated from CTRATE dataset with RadBERT Classifier**

Report Findings	Medical material	Arterial wall calcification	Cardiomegaly	Pericardial effusion	Coronary artery wall calcification	Hiatal hernia	Lymphadenopathy	Emphysema	Atelectasis	Lung nodule	Lung opacity	Pulmonary fibrotic sequela	Pleural effusion	Mosaic attenuation pattern	Peribronchial thickening	Consolidation	Bronchietasis	Interlobular septal thickening
Trachea, both main bronchi are open and no occlusive pathology is detected. No pathological increase in wall thickness was observed in the thoracic esophagus. There are calcific atherosomatous plaques in the aorta and left coronary artery. No pericardial or pleural effusion was detected. Calibration of other mediastinal vascular structures, heart contour, size are normal. No lymph node in pathological size and appearance was observed in the mediastinum. In the examination made in the lung parenchyma window; No active infiltration or mass lesion was detected in both lungs. There are minimal emphysematous changes. No lytic-destructive lesion was detected in the bone structures within the image. There are degenerative changes.		0	1	0	0	1	0	0	1	0	0	0	0	0	0	0	0	0
Trachea and main bronchi are open. No pathological lymph node was detected in the mediastinum. The heart and mediastinal vascular structures have a natural appearance. Esophagus is within normal limits. Pleural effusion-thickening was not detected in both hemithorax. In the evaluation of both lung parenchyma; No suspicious mass, nodule or infiltration was detected in both lungs. In the sections passing through the upper part of the abdomen, the bilateral adrenal glands appear natural. No significant pathology was detected in the abdominal sections. No obvious pathology was detected in bone structures.		0	0	0	0	0	0	0	0	0	0	0	0	0	0	0	0	0

*Figure 2: Examples of generated reference standard labels from MIMIC-CXR, and CT-RATE datasets using ChexBERT, and RadBERT models respectively. For CheXbert, the primary multi-class labels have been converted to a binary (present/absent) format to align with the classification task. The top row shows the initial CheXbert outputs, while the bottom row displays the binarized labels, whereas the primary labels generated by RadBERT are binary. For both CheXbert and RadBERT, we present two sample report findings alongside their corresponding classification results.*

**Differentially Private Fine-Tuning:** In this Section, we describe the concept of Differential Privacy (DP) adapted for fine-tuning LLMs on patient data. Intuitively, DP ensures that the fine-tuned LLM does not reveal whether any specific example, for instance, a patient report was part of its training data, even if an adversary analyzes the model and its behavior very carefully. This captures the core idea that no individual patient’s training data leaves a noticeable imprint on the resulting fine-tuned LLM. We next provide the formal definition of DP.

**$(\epsilon, \delta)$ -Differential Privacy** [1] [2] : For all pairs of neighboring training datasets  $D$  and  $D'$  that differ by a single patient's data, i.e.,  $|D - D'| \leq 1$ , a randomized fine-tuning algorithm  $M$  with an input domain of  $X$  and output range  $R$  is considered to be  $(\epsilon, \delta)$ -differentially private, if  $\forall S \subseteq R$ :

$$Pr[M(D) \in S] \leq \exp(\epsilon) \cdot Pr[M(D') \in S] + \delta.$$

This definition ensures that the distributions of LLMs fine-tuned on datasets differing by one individual patient's data –  $M(D)$  and  $M(D')$  are statistically similar, making it harder to tell whether any single patient's data was used in fine-tuning. The closeness between  $M(D)$  and  $M(D')$  is controlled by the **privacy budget** ( $\epsilon$ ); smaller  $\epsilon$  means stronger privacy. The parameter  $\delta$  allows for a small probability of failure i.e., with probability at most  $\delta$ , the privacy guarantee of  $\epsilon$  might not hold.

**Selection of privacy parameters  $(\epsilon, \delta)$ :** The selection of the privacy budget ( $\epsilon$ ) and the failure probability ( $\delta$ ), therefore plays a critical role in the privacy-utility trade-off. Strong privacy guarantees are achieved by keeping both  $\epsilon$  and  $\delta$  as small as possible [24]. In healthcare, and other high stakes domain, keeping the value of  $\epsilon$  between  $(0, 10)$  is common practice to ensure robust protection. An appropriate choice for the parameter  $\delta$  is  $1/n^2$  where  $n$  denotes the number of training samples used for fine-tuning. This choice of  $\delta$  ensures the probability of privacy failure is vanishingly small as the dataset size grows.

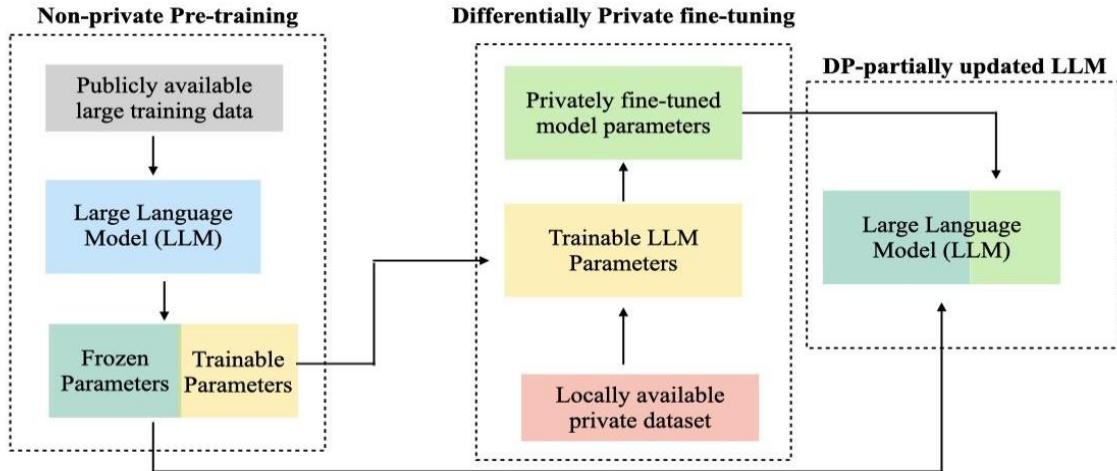


Figure 3: Differentially private fine-tuning updates only a subset of low-rank model parameters on local medical data, while keeping the rest of the pre-trained LLM frozen.

**DP-Low Rank Adaptation (DP-LoRA) :** LoRA [3] is a parameter-efficient fine-tuning technique that avoids updating the full weight matrix  $W_p \in R^{\{d \times k\}}$ , instead, it freezes the original weights and introduces a low-rank decomposition  $W_p + \Delta W_p = W_p + B \cdot A$  where  $B \in R^{\{d \times r\}}$ ,  $A \in R^{\{r \times k\}}$  and the rank  $r \leq \min(d, k)$ . The weight matrix  $W_p$  maps to attention projections, and LoRA fine-tunes these layers by updating only the low-rank matrices  $A$  and  $B$ , while the original weights remain fixed and do not receive gradient updates. The gradients are computed with respect to a task-specific loss function, which guides parameter updates during the fine-tuning process.

To ensure differential privacy during fine-tuning, we incorporate DP-SGD [20], which privately modifies the gradients of the trainable parameters [19]. At each update step, gradients are first clipped to a predefined norm bound  $C$  to limit sensitivity. Then, Gaussian noise with zero mean and standard deviation  $\sigma = \sqrt{1.25 \log(I/\delta)}/\epsilon$  is added to the clipped gradients to achieve  $(\epsilon, \delta)$ -DP.

### **Results:**

In this Section, we first highlight the text-memorization on GPT2 and BERT-base models in Figure 4. Then we present the results on private and non-private fine-tuning of 3 different models on 2 different datasets. Specifically, we present the experimental results on the MIMIC-CXR and CT-RATE datasets with 3 models of different sizes: BERT-medium (41.7M parameters), BERT-small (29.1M parameters) [25], and ALBERT-base-v2 (11M parameters) [26]. For the scope of this paper we have considered the weighted F1-score [6] metric while reporting the predictive performance of the fine-tuned models with and without differential privacy. To evaluate model performance in the presence of class imbalance, we use the weighted F1-score, a metric that computes the F1-score for each class and averages them according to their support (i.e., the number of true instances per class). Since the labels are highly imbalanced, we have used the weighted F1-score that considers both the correctly predicted positive labels (+1) and negative labels (0).

**Reference Standard Text-Report:** Retropectoral breast implant with bilateral extracapsular rupture was observed. In the bilateral axilla, there are multiple lymphadenopathy with thick cortex, the largest of which is 24x17 mm on the right. After infection, it should be evaluated under elective conditions. Trachea and main bronchi are open. No pathological lymph node was detected in the mediastinum. The heart and mediastinal vascular structures have a natural appearance. Esophagus is within normal limits. Pleural effusion-thickening was not detected in both hemithorax. In the evaluation of both lung parenchyma; No suspicious mass, nodule or infiltration was detected in both lungs. There are millimetric non-specific nodules in the bilateral lung. In the sections passing through the upper part of the abdomen, the bilateral adrenal glands appear natural. No significant pathology was detected in the abdominal sections. No obvious pathology was detected in bone structures.

**Prompt:** Complete the text "Retropectoral breast implant with bilateral extracapsular rupture was observed. In the bilateral axilla, there are multiple lymphadenopathy with thick cortex, the largest of which is "

### Fine-tuned model response

### Off-the-shelf non-fine-tuned model

GPT2-  
large

Retropectoral breast implant with bilateral extracapsular rupture was observed. In the bilateral axilla, there are multiple lymphadenopathy with thick cortex, the largest of which is iliac arteries and measures 24x17 mm. Heart contour and size are normal. No pleural-pericardial effusion or thickening was detected. The widths of the mediastinal main vascular structures are normal. No enlarged lymph node was detected in the mediastinum and bilateral hilar regions in pathological size and appearance. Trachea and both main bronchi are open. No occlusive pathology was detected in the trachea and both main bronchi. There is bilateral tubular bronchiectasis. There are areas of atelectasis in the left lung upper lobe lingular segment inferior subsegment and right lung middle lobe medial segment. No mass or infiltrative lesion was observed in both lungs. There are areas of linear atelectasis in the left lung.

(a)

**Reference Standard Text Report:** PA and lateral views of the chest are obtained. There is a mild pectus deformity noted on the lateral view. The lungs appear well expanded without focal consolidation, effusion, or pneumothorax. No definite signs of CHF. The heart size appears slightly prominent, but this could be due to the aforementioned pectus excavatum deformity. Imaged osseous structures are intact. Clips in the right upper quadrant noted.

- No Fine-Tuning
- Non Private Fine-Tuning

**PROMPT:** PA and lateral views of the chest are obtained. There is a mild pectus deformity noted on the lateral view. The lungs appear well expanded without focal consolidation, effusion, or pneumothorax. No definite signs of CHF. The heart size appears slightly prominent, but this could be due to the aforementioned pectus excavatum deformity. Imaged osseous structures are [MASK] [MASK] [MASK] [MASK] [MASK] [MASK] [MASK] [MASK] [MASK] [MASK].

### Non-fine-tuned model response

pa and lateral views of the chest are obtained . there is a mild pectus deformity noted on the lateral view . the lungs appear well expanded without focal consolidation , effusion , or pneumothorax . no definite signs of chf . the heart size appears slightly prominent , but this could be due to the aforementioned pectus excavatum deformity . imaged osseous structures are " " , " " , " " , etc .

### Fine-tuned model response

PA and lateral views of the chest are obtained . there is a mild pectus deformity noted on the lateral view . the lungs appear well expanded without focal consolidation , effusion , or pneumothorax . no definite signs of chf . the heart size appears slightly prominent , but this could be due to the aforementioned pectus excavatum deformity . imaged osseous structures are grossly intact . impression : mild severe edema.

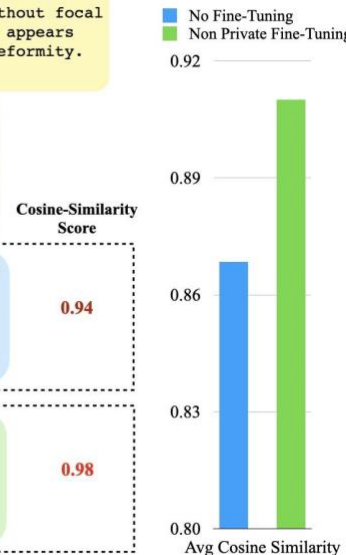


Figure 4: (a) Memorization behavior of the GPT-2 Large model on text-based radiology reports reveals that, during report completion tasks, the model can recall and reproduce patient-specific numerical values (e.g.,  $24 \times 17 \text{ mm}$ ) from its training data, thereby amplifying privacy risks. (b) Example illustrates rising Cosine similarity between original report Findings and BERT-base-generated Findings, indicating memorization even in non-causal models, more pronounced in the fine-tuned variant.

**Text-memorization illustration by LLMs:** As highlighted in the Introduction Section, fine-tuning LLMs can pose significant privacy risks when models are exposed to real patient data. In Figure 4, we illustrate these threats via text-memorization using GPT2 (causal language model), BERT, and ALBERT (abnormality classification models), and show how these fine-tuned LLMs can memorize patient data. Our findings show fine-tuned LLMs reflect memorized training content compared to the off-the-shelf (non-fine-tuned) LLM, this indicates that fine-tuned models exhibit especially strong tendencies toward such leakage. As shown in Figure 4 (a), when asked to complete a partial report, fine-tuned GPT2 models were able to replicate parts of the original report “Findings”. Moreover, we observe that the fine-tuned model outputs specific numeric values from the fine-tuning dataset, highlighting the privacy vulnerabilities of non-privately fine-tuned LLMs.

In Figure 4 (b), we observe a similar trend for fine-tuned BERT and ALBERT models. It is interesting to note that BERT based models are not causal language models, yet they still have the ability to replicate portions of reports used for fine-tuning. Specifically, the fine-tuned models achieved a higher cosine similarity score (between generated and original report “*Findings*”) compared to non-fine-tuned ones. Cosine similarity score measures how similar two pieces of text are by comparing the angle between their vector representations in the embedding space; a higher cosine similarity between generated text and the original training data suggests the model may be closely repeating what it saw during training, indicating memorization. This underscores the potential privacy risks posed by LLMs memorizing sensitive portions of medical reports, especially when applied to tasks such as text completion, disease classification, report summarization, and more.

**Effect of DP on classification performance:** In this experimental section, we compare the effect of differentially private fine-tuning in different privacy regimes compared to the non-fine-tuned models and models fine-tuned without any privacy constraints.

Dataset	Model	non-FT (off the shelf model)	Privacy Budget ( $\epsilon$ )				Non-priv LoRA (r = 64)	Non-priv Full FT
			0.01	0.1	1	10		
MIMIC-CXR	ALBERT-base	$0.515 \pm 0.274$	$0.539 \pm 0.307$	$0.834 \pm 0.126$	$0.886 \pm 0.071$	$0.89 \pm 0.061$	$0.892 \pm 0.064$	$0.965 \pm 0.017$
	BERT-small	$0.523 \pm 0.298$	$0.372 \pm 0.167$	$0.48 \pm 0.046$	$0.89 \pm 0.062$	$0.898 \pm 0.055$	$0.901 \pm 0.066$	$0.967 \pm 0.018$
	BERT-medium	$0.527 \pm 0.31$	$0.395 \pm 0.122$	$0.47 \pm 0.025$	$0.883 \pm 0.073$	$0.901 \pm 0.053$	$0.91 \pm 0.072$	$0.968 \pm 0.019$
CTRATE	ALBERT-base	$0.461 \pm 0.315$	$0.315 \pm 0.164$	$0.45 \pm 0.028$	$0.492 \pm 0.051$	$0.591 \pm 0.123$	$0.788 \pm 0.111$	$0.972 \pm 0.018$
	BERT-small	$0.384 \pm 0.279$	$0.358 \pm 0.162$	$0.448 \pm 0.033$	$0.479 \pm 0.049$	$0.537 \pm 0.099$	$0.795 \pm 0.112$	$0.971 \pm 0.018$
	BERT-medium	$0.390 \pm 0.329$	$0.315 \pm 0.162$	$0.449 \pm 0.032$	$0.477 \pm 0.044$	$0.535 \pm 0.10$	$0.792 \pm 0.117$	$0.972 \pm 0.018$

Table 1: This table shows the mean and standard deviation of the weighted F1-score (over 10 epochs) of 3 models BERT-small, BERT-medium, and ALBERT-base over different privacy regimes with four different privacy budgets  $\epsilon = (0.01, 0.1, 1.0, 10.0)$ . This shows the privacy-utility trade-off in different privacy regimes.

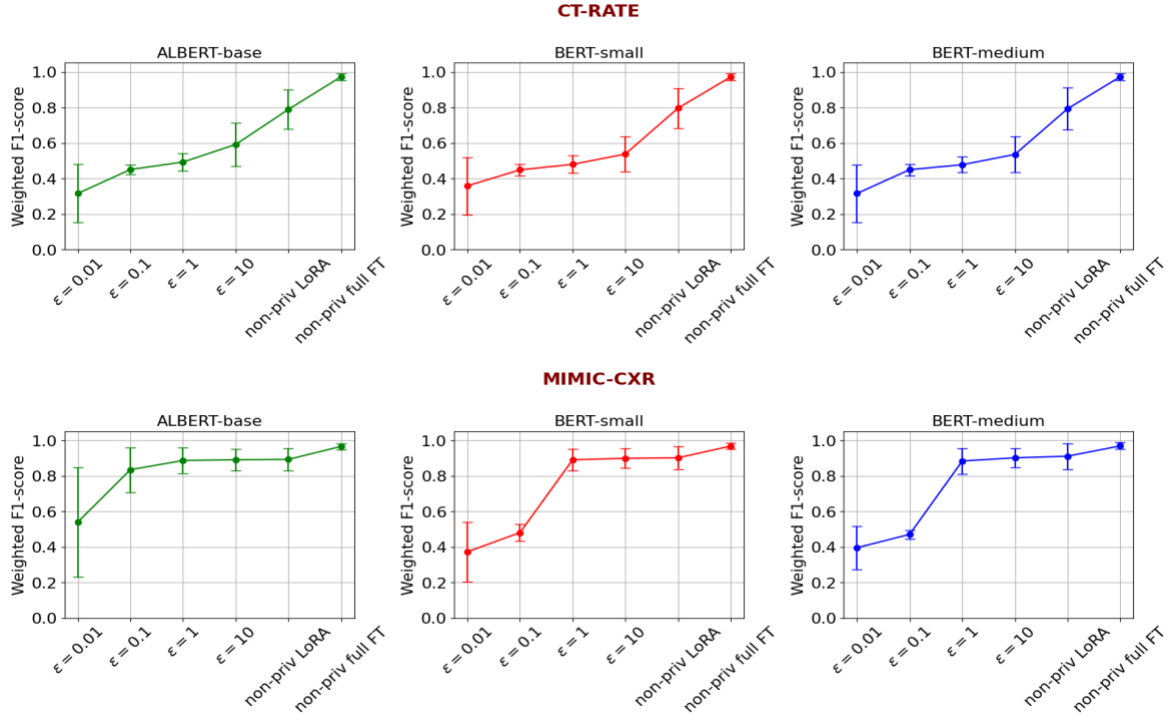


Figure 5: Privacy-utility tradeoff for ALBERT-base, BERT-small and BERT-medium models across varied privacy regimes. As the privacy budgets increase, due to less stringent privacy constraints, the model utility increases.

From Table 1 and Figure 5, we observe that the performance of ALBERT-base, BERT-small, and BERT-medium models across different training conditions, including off-the-shelf (non-fine-tuned), differential privacy (DP-SGD) with varying epsilon values, and non-private fine-tuning methods. When fine-tuned with DP-SGD, the models show improved performance for both the datasets, as epsilon increases, indicating a clear privacy-utility tradeoff. In contrast, non-private fine-tuning significantly boosts accuracy: on MIMIC-CXR, non-private LoRA achieves 0.901 for BERT models and 0.891 for ALBERT-base, while full fine-tuning results in the highest accuracy across all models, with BERT-medium reaching 0.968. On CT-RATE dataset, the non-private LoRA achieves  $\sim 0.79$  F1-score whereas the non-private full fine-tuning achieves 0.97. Overall, full fine-tuning without privacy provides the best performance, while DP-SGD enables comparable F1-score with strong privacy guarantees. We observe a higher F1-score on the MIMIC-CXR dataset compared to CT-RATE, primarily due to two factors. First, the reference standard labels for MIMIC-CXR were generated using CheXbert, a BERT-based model fine-tuned on the MIMIC dataset, which aligns closely with the domain and structure of the test data. Second, CT reports tend to be longer and more complex than CXR reports, introducing additional linguistic and semantic challenges for automated label extraction.

**Effect of LoRA Rank on Utility:** Intuitively, as we increase the LoRA ranks, the predictive performance of the models gets better, achieving significantly better F1-scores.

Dataset	Models	<b>r = 1</b>	<b>r = 32</b>	<b>r = 64</b>	<b>r = 128</b>
MIMIC-CXR	ALBERT- base	$0.824 \pm 0.137$	$0.88 \pm 0.076$	$0.886 \pm 0.069$	$0.893 \pm 0.060$
	BERT- small	$0.901 \pm 0.054$	$0.892 \pm 0.061$	$0.890 \pm 0.062$	$0.881 \pm 0.074$
	BERT- medium	$0.890 \pm 0.062$	$0.891 \pm 0.061$	$0.883 \pm 0.073$	$0.881 \pm 0.072$
CT-RATE	ALBERT- base	$0.448 \pm 0.033$	$0.496 \pm 0.051$	$0.492 \pm 0.051$	$0.516 \pm 0.090$
	BERT- small	$0.531 \pm 0.137$	$0.498 \pm 0.063$	$0.479 \pm 0.049$	$0.472 \pm 0.033$
	BERT- medium	$0.527 \pm 0.100$	$0.499 \pm 0.068$	$0.477 \pm 0.044$	$0.474 \pm 0.042$

*Table 2: This table represents the predictive performance of 3 models ALBERT-base, BERT-small, and BERT-medium for a fixed privacy budget of  $\epsilon = 1.0$ , and DP-failure probability of  $\delta$  for varied LoRA ranks (i.e., number of fine-tuned parameters).*

The results in Table 2 highlight the critical role of LoRA rank ( $r$ ) in navigating the privacy-utility trade-off during LLM fine-tuning. Under a fixed total privacy budget, increasing the LoRA rank ( $r$ ) leads to a proportional increase in the number of trainable parameters. As a result, more noise must be added per training step to satisfy differential privacy constraints, which in turn degrades the model’s predictive performance, most notably reflected in lower F1 scores. This demonstrates that the choice of LoRA rank is not merely a tuning parameter but a key factor in balancing model utility and privacy. Careful calibration of the rank is therefore essential to optimize performance under stringent privacy guarantees.

#### **Discussion:**

LLMs offer a scalable and efficient solution for parsing free-text radiology reports, enabling both structured data extraction and multi-abnormality labeling. These capabilities are essential for building high-quality labeled datasets and improving the efficiency of downstream diagnostic tasks, especially, the tasks that are otherwise difficult to scale through manual annotation alone. This work adopts a framework for optimizing the fine-tuning of large language models (LLMs) with differential privacy (DP) guarantees for multi-abnormality classification from free-text radiology reports. Our proposed approach addresses the privacy utility trade-off in LLMs within the healthcare domain, particularly for radiology-based multi-abnormality classification, by integrating Low-Rank Adaptation (LoRA) with differential privacy techniques. Through extensive experimentation on free-text radiology reports from MIMIC-CXR and CT-RATE datasets, we demonstrate that our DP-LoRA framework achieves strong classification performance under rigorous privacy constraints. We compare our results with the recent prior work [6] which developed a fine-tuning framework for LLMs using similar datasets without any privacy consideration. We observe that our proposed privacy preserving fine-tuning framework for multi-abnormality classification achieves a comparable weighted F1-score along with rigorous DP guarantees. We explore the effects of different privacy budgets, LoRA ranks, and their interplay on the classification performance via F1-score. The main contribution of this work lies in analyzing the trade-off between privacy and utility while fine-tuning LLMs with DP. Our findings reveal that guaranteeing DP inevitably leads to some loss in classification utility, and the extent of this degradation depends on multiple factors, including the chosen privacy budget and

LoRA rank. Notably, models fine-tuned with more relaxed privacy settings (i.e., larger privacy budgets) achieved higher utility in terms of weighted F1 scores. However, this performance gain comes at the expense of reduced privacy, as reflected in increased prediction variability and heightened risks of potential data leakage.

Our experiments show a strong dependency between the number of model parameters updated during fine-tuning and downstream predictive performance. In non-private settings, increasing the number of parameters (i.e., increasing the LoRA rank), corresponding to higher fine-tuning capacity consistently improves the weighted F1 scores. However, under strict differential privacy constraints, the benefits of tuning more parameters will reduce due to the higher amount of noise required for privacy. These findings highlight the importance of carefully calibrating key hyperparameters, particularly the number of trainable weights and privacy budgets, to achieve an optimal trade-off between utility and privacy. Future research includes exploration strategies that promote generalization, especially for imbalanced datasets and abnormality categories, while preserving strong privacy guarantees. Potential directions include techniques such as class reweighting and label smoothing under privacy constraints. Our findings also support the practical viability of deploying lightweight models in clinical workflows. By differentially privately fine-tuning compact architectures such as BERT-small, we maintain competitive predictive performance while satisfying the computational efficiency and data confidentiality requirements critical for real-world healthcare applications.

We now outline some limitations of this study and suggest directions for future research to address them and extend our findings. First, while we demonstrate the effectiveness of our approach on chest X-ray-based free-text reports, its generalizability remains unexplored across broader clinical contexts and multi-modal data. Future work should evaluate the framework on more diverse datasets representing varied patient populations and imaging modalities. Second, although this study does not explicitly address adversarial attack strategies in LLM-based healthcare applications, understanding and mitigating such risks remains a critical challenge for real-world deployment. In future work, we plan to systematically investigate privacy vulnerabilities in vision-language models (VLLMs) and contrastive learning frameworks,

particularly in the context of multi-modal medical data analysis, where text and imaging data are jointly leveraged. Third, our implementation relies on standard differential privacy techniques, such as Differentially Private Stochastic Gradient Descent (DP-SGD) and Gaussian Mechanism. More advanced approaches, such as adaptive privacy budgeting or alternative noise distributions, may offer improved privacy-utility trade-offs and merit further exploration.

### **Conclusions:**

Our research presents a differential privacy-preserving fine-tuning framework for multi-abnormality classification tasks from text-radiology reports that can be easily adapted for other text-based healthcare-related tasks. Through comprehensive experimental results, we demonstrate that it is simultaneously possible to achieve both strong privacy protection and competitive performance on multi-abnormality classification tasks through a differentially private fine-tuning framework that incorporates Low Rank Adaptation. The proposed framework is versatile and can be extended to a range of applications, including multi-organ multi-abnormality classification, multi-modal medical data analysis, report generation - summarization, and other classification tasks. As part of our future work, we plan to conduct an in-depth analysis of privacy vulnerabilities and explore robust privacy-preserving strategies tailored to multi-organ, multi-abnormality classification using multi-modal datasets.

**References:**

- [1] C. Dwork and A. Roth, “The Algorithmic Foundations of Differential Privacy,” *Found. Trends® Theor. Comput. Sci.*, vol. 9, no. 3–4, pp. 211–407, 2013, doi: 10.1561/0400000042.
- [2] C. Dwork, F. McSherry, K. Nissim, and A. Smith, “Calibrating Noise to Sensitivity in Private Data Analysis,” in *Theory of Cryptography*, S. Halevi and T. Rabin, Eds., in Lecture Notes in Computer Science. Berlin, Heidelberg: Springer, 2006, pp. 265–284. doi: 10.1007/11681878\_14.
- [3] E. J. Hu *et al.*, “LoRA: Low-Rank Adaptation of Large Language Models,” Oct. 16, 2021, *arXiv*: arXiv:2106.09685. doi: 10.48550/arXiv.2106.09685.
- [4] Y. Li, S. Wang, H. Ding, and H. Chen, “Large Language Models in Finance: A Survey,” Jul. 08, 2024, *arXiv*: arXiv:2311.10723. doi: 10.48550/arXiv.2311.10723.
- [5] S. Wang *et al.*, “Large Language Models for Education: A Survey and Outlook,” Apr. 01, 2024, *arXiv*: arXiv:2403.18105. doi: 10.48550/arXiv.2403.18105.
- [6] E. Erberk Uslu, E. Sezer, and Z. Anil Guven, “NLP-Powered Healthcare Insights: A Comparative Analysis for Multi-Labeling Classification With MIMIC-CXR Dataset,” *IEEE Access*, vol. 12, pp. 67314–67324, 2024, doi: 10.1109/ACCESS.2024.3400007.
- [7] K. He *et al.*, “A survey of large language models for healthcare: from data, technology, and applications to accountability and ethics,” *Inf. Fusion*, vol. 118, p. 102963, Jun. 2025, doi: 10.1016/j.inffus.2025.102963.
- [8] Y. Liu, “Fine-tune BERT for Extractive Summarization,” Sep. 05, 2019, *arXiv*: arXiv:1903.10318. doi: 10.48550/arXiv.1903.10318.
- [9] J. Devlin, M.-W. Chang, K. Lee, and K. Toutanova, “BERT: Pre-training of Deep Bidirectional Transformers for Language Understanding,” May 24, 2019, *arXiv*: arXiv:1810.04805. doi: 10.48550/arXiv.1810.04805.
- [10] J. Lee *et al.*, “BioBERT: a pre-trained biomedical language representation model for biomedical text mining,” *Bioinformatics*, vol. 36, no. 4, pp. 1234–1240, Feb. 2020, doi: 10.1093/bioinformatics/btz682.

[11] N. Kaur and A. Mittal, “RadioBERT: A deep learning-based system for medical report generation from chest X-ray images using contextual embeddings,” *J. Biomed. Inform.*, vol. 135, p. 104220, Nov. 2022, doi: 10.1016/j.jbi.2022.104220.

[12] X. Cai, S. Liu, J. Han, L. Yang, Z. Liu, and T. Liu, “ChestXRayBERT: A Pretrained Language Model for Chest Radiology Report Summarization,” *IEEE Trans. Multimed.*, vol. 25, pp. 845–855, 2023, doi: 10.1109/TMM.2021.3132724.

[13] A. Smit, S. Jain, P. Rajpurkar, A. Pareek, A. Y. Ng, and M. P. Lungren, “CheXbert: Combining Automatic Labelers and Expert Annotations for Accurate Radiology Report Labeling Using BERT,” Oct. 18, 2020, *arXiv*: arXiv:2004.09167. doi: 10.48550/arXiv.2004.09167.

[14] P. Mukherjee, B. Hou, R. B. Lanfredi, and R. M. Summers, “Feasibility of Using the Privacy-preserving Large Language Model Vicuna for Labeling Radiology Reports,” *Radiology*, vol. 309, no. 1, p. e231147, Oct. 2023, doi: 10.1148/radiol.231147.

[15] N. Carlini *et al.*, “Extracting Training Data from Large Language Models”.

[16] M. Duan *et al.*, “Do Membership Inference Attacks Work on Large Language Models?,” Sep. 16, 2024, *arXiv*: arXiv:2402.07841. doi: 10.48550/arXiv.2402.07841.

[17] T. Akinci D’Antonoli *et al.*, “Cybersecurity Threats and Mitigation Strategies for Large Language Models in Health Care,” *Radiol. Artif. Intell.*, p. e240739, May 2025, doi: 10.1148/ryai.240739.

[18] J. Hong, J. T. Wang, C. Zhang, Z. Li, B. Li, and Z. Wang, “DP-OPT: Make Large Language Model Your Privacy-Preserving Prompt Engineer,” Mar. 17, 2024, *arXiv*: arXiv:2312.03724. doi: 10.48550/arXiv.2312.03724.

[19] X.-Y. Liu *et al.*, “Differentially Private Low-Rank Adaptation of Large Language Model Using Federated Learning,” Jun. 02, 2024, *arXiv*: arXiv:2312.17493. doi: 10.48550/arXiv.2312.17493.

[20] M. Abadi *et al.*, “Deep Learning with Differential Privacy,” in *Proceedings of the 2016 ACM SIGSAC Conference on Computer and Communications Security*, Oct. 2016, pp. 308–318. doi: 10.1145/2976749.2978318.

[21] A. E. W. Johnson *et al.*, “MIMIC-CXR, a de-identified publicly available database of chest

radiographs with free-text reports,” *Sci. Data*, vol. 6, no. 1, p. 317, Dec. 2019, doi: 10.1038/s41597-019-0322-0.

[22] I. E. Hamamci *et al.*, “Developing Generalist Foundation Models from a Multimodal Dataset for 3D Computed Tomography,” Apr. 04, 2025, *arXiv*: arXiv:2403.17834. doi: 10.48550/arXiv.2403.17834.

[23] A. Yan *et al.*, “RadBERT: Adapting Transformer-based Language Models to Radiology,” *Radiol. Artif. Intell.*, vol. 4, no. 4, p. e210258, Jul. 2022, doi: 10.1148/ryai.210258.

[24] J. Hsu *et al.*, “Differential Privacy: An Economic Method for Choosing Epsilon,” in *2014 IEEE 27th Computer Security Foundations Symposium*, Vienna: IEEE, Jul. 2014, pp. 398–410. doi: 10.1109/CSF.2014.35.

[25] I. Turc, M.-W. Chang, K. Lee, and K. Toutanova, “Well-Read Students Learn Better: On the Importance of Pre-training Compact Models,” Sep. 25, 2019, *arXiv*: arXiv:1908.08962. doi: 10.48550/arXiv.1908.08962.

[26] Z. Lan, M. Chen, S. Goodman, K. Gimpel, P. Sharma, and R. Soricut, “ALBERT: A Lite BERT for Self-supervised Learning of Language Representations,” Feb. 09, 2020, *arXiv*: arXiv:1909.11942. doi: 10.48550/arXiv.1909.11942.